Cosmic Ray Composition Measurement between 3 PeV to 30 PeV with the TALE Hybrid Detector

Keitaro Fujita[a,*] **on behalf of the Telescope Array Collaboration**

[a]*Institute for Cosmic Ray Research, the University of Tokyo,*
5-1-5 Kashiwa-no-Ha, Kashiwa, Chiba, Japan

E-mail: kfujita@icrr.u-tokyo.ac.jp

We report on the cosmic ray mass composition measured by the Telescope Array Low-energy Extension (TALE) hybrid detector. The TALE detector began operations in 2017 with 10 high-elevation fluorescence telescopes and a surface detector (SD) array of 80 scintillation counters, including 40 with 400 m spacing and 40 with 600 m spacing. In 2023, we constructed a new array made up of 50 SDs with a spacing of 100 m to lower the energy threshold of hybrid mode down to PeV range for the investigation of the cosmic ray mass composition around knee structure in the spectrum. Here we will present an estimate of the performance of the hybrid mode which is a combination of the new SD array and TALE-FD using a Monte Carlo simulation, and report the first preliminary results of the mass composition measurement using the new hybrid detector.

---

*Speaker

1. Introduction

Cosmic rays in the PeV to EeV energy range play a key role in understanding their acceleration and propagation mechanisms in our galaxy. This region includes the well-known "knee" [1] at a few PeV, where the spectrum steepens, and the "second knee", marking further steepens. Precise measurements of composition are critical for constraining theoretical models.

The Telescope Array Low-Energy Extension (TALE) extends the capabilities of the Telescope Array (TA) experiment, enabling observations of cosmic rays down to PeV energies. The hybrid observation mode, which combines the fluorescence detectors (FD) and surface detectors (SD) array, provides improved energy and X_{max} reconstruction compared to the monocular mode. Ten high-elevation telescopes, covering a field of view of 31° to 59° in elevation angle. Each telescope has 256-pixel photomultiplier tubes, operating with 8- bit 10 MHz FADC readout [2]. Observations have started since 2013. The SD array comprises 80 scintillation counters. Each counter consists of two layers of scintillators with an area of 3 m². 40 counters are deployed in the forward direction of the FD field of view with a spacing of 400 m, while the remaining 40 counters are spaced at 600 m. This SD array activates an air shower trigger when any four or more detectors record signals equivalent to three or more particles

Figure 1: TALE detector layout (SD: □, FD: ●). The configuration of the new SDs with a spacing of 100 m is shown in the upper panel.

within a time window of 32 μs. The array configuration is shown at the bottom of Figure 1. Observations began in 2018. In addition, a new dense array of 50 scintillation counters with 100 m spacing was deployed between the original SD array and FD position as shown in the upper panel of Figure 1 in October 2022, and began the observation in November 2023. For this new array, we set the air shower trigger which activates when adjacent five or mode detectors record signals equivalent to three or more particles within a time window of 3 μs. This setup ensures reliable detection of extensive air showers while minimizing false triggers from random background events. The operation duty cycle of the new SD array exceeds 98% as shown in Figure 2a. The accumulated number of recorded triggering events by the SD array had reached approximately ten million just before the conference, as indicated by the solid line in Figure 2a. Also, 540 hours of hybrid observation data had been accumulated by the end of June 2024 as shown in Figure 2b and is used in this work.
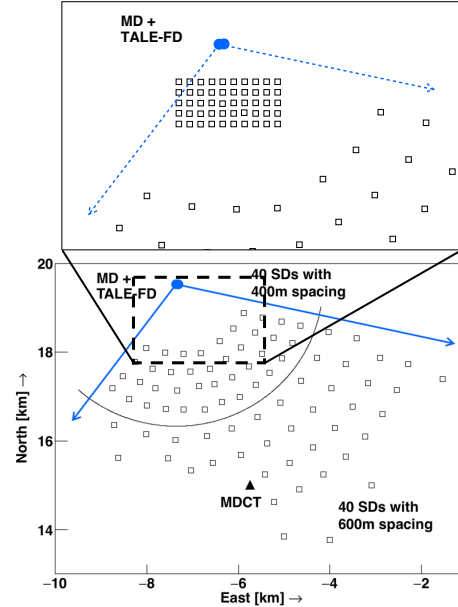
2. Event Reconstruction

The event reconstruction is basically the same as our previous work in [4] except for one point. In the previous hybrid geometry reconstruction, even when multiple SDs detected air shower signals,
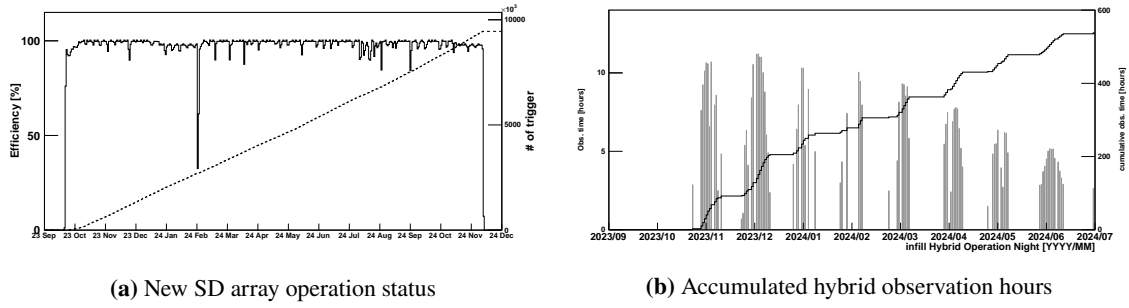
(a) New SD array operation status

(b) Accumulated hybrid observation hours

Figure 2: The operation status summary. Left: The histogram shows the efficiency defined as the number of SD in operation over the maximum number of SD for every 10 minutes. Right: Accumulated hybrid observation time is shown by the solid line. The gray histogram represents observation hours per day.

only the position and timing information from a single SD, combined with FD tube timings, were used to determine the shower axis. However events with the new SD array have larger footprints of air showers as shown in the left panel of Figure 3, so the hybrid geometry reconstruction has been updated to constrain the shower core using lateral fits of the SD array signals. Specifically, the chi-squared (χ^2) value from the FD tube timings is combined with the χ^2 value derived from the shower core determined by the SD lateral fit, and the total χ^2 is minimized in the reconstruction process. This update allows the shower core to be determined with a resolution of 10 m, even for shower energy as low as $10^{15.5}$ eV. The arrival direction is also determined with a precision of $0.5°$. Consequently, the energy and $X_{\max}$ values can be reconstructed with resolutions of $< 10\%$ and < 25 g/cm^2, respectively, as summarized in Table 1.

Table 1: Resolution achieved by the combination of TALE FD and new SD hybrid mode.

Parameter	Resolution
R_p (Impact Parameter)	10 m
ψ (Angle)	$0.5°$
$X_{\max}$	< 25 g/cm^2
Energy	$< 10\%$

3. Data and Monte Carlo Comparisons

We run the Monte Carlo simulations to evaluate our detector performance and reconstruction resolution. In this work, we generated proton and iron cosmic rays air showers using CORSIKA [5] air shower simulation tool with the hadronic interaction model of QGSJetII-04 [6]. Equal numbers of events were generated for each primary type. The generated MC events follow a broken power law spectrum in which the spectrum index is -2.7 below $10^{15.6}$ eV and is -3.0 above the break energy, where each parameter comes from recently reported by LHAASO collaboration [7]. All of the calibration factors with time dependence are considered in the SD and FD detector simulations. To ensure the quality of reconstructed events and to avoid potential $X_{\max}$ biases and resolution degradation, the following event selection criteria are applied:
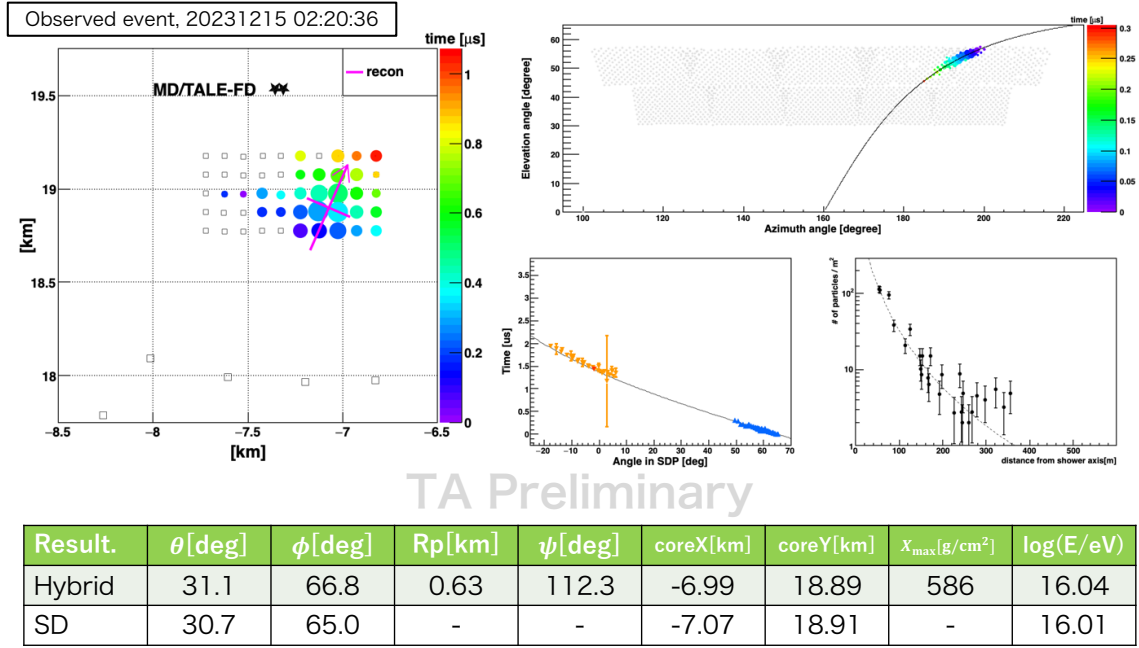
Figure 3: Event example observed by the combination of the TALE FD and new SD array hybrid mode. The triggered SDs are shown in the left panel. Marker radius is proportional to the signal size measured by the SD, and color indicates trigger time. The arrow shows the reconstructed azimuthal angle of the shower direction, and the crossed point corresponds to the reconstructed shower core position. The top-right panel shows the shower track of this hybrid event as seen by the fluorescence telescopes. Marker radius indicates signal size, and color indicates trigger time. The solid line is the shower-detector plane found by reconstruction. The bottom-middle panel shows the result of hybrid geometry fit. The inverted triangles show the trigger time and viewing angle of FD PMTs that observed the passage of the shower. The inverted triangles show the same information for SDs. The reconstructed lateral distribution of this shower is shown in the bottom-right panel. Reconstructed shower parameters obtained by hybrid mode and only by SD array [3] are summarized in the bottom table.

- Successful reconstruction of shower geometry and profile.
- Observations made under good weather conditions.
- X_{max} observed within the field of view of the FDs.
- Total number of photo-electrons exceeds 1000.
- Ratio of photo-electrons to the number of hit PMTs exceeds 50.
- FD event duration longer than 100 ns.
- Minimum viewing angle, defined as the angle between the shower axis and the pixel field of view direction, exceeds $1.5°$.
- Distance between the reconstructed shower axis and the SD with the largest signal is less than 100 m.
- Number of PMTs at the edge of the FD field of view is fewer than five.
- The brightest PMT is not located at the edge of the FD field of view.

After the event selections have been applied to the experimental data, 8978 events remain within the energy range of $10^{15.5}$ to $10^{16.4}$ eV. The results of the comparisons of experimental data and Monte

Result.	θ[deg]	ϕ[deg]	Rp[km]	ψ[deg]	coreX[km]	coreY[km]	X_{max}[g/cm²]	log(E/eV)
Hybrid	31.1	66.8	0.63	112.3	-6.99	18.89	586	16.04
SD	30.7	65.0	-	-	-7.07	18.91	-	16.01

Carlo events are displayed in Figure 4. The number of PMTs in shower track (Figure. 4a), the number of photo-electrons (Figure. 4b), the impact parameter, R_p (Figure. 4c), the shower inclination angle in the SDP ψ (Figure. 4d), $s50$ which is the energy estimator of SD reconstruction (see details in [3]) (Figure. 4e) and the number of SD in cluster coincided with space and timing are displayed. In the comparisons, we split the dataset with reconstructed energy at $E = 10^{16}$ eV. All MC histograms are normalized by the entries of experimental data. We found the data and MC histograms comparison shows good agreement.

(a) number of PMTs   **(b)** number of photo-electrons

(c) Shower impact parameter, R_p **(d)** ψ angle

(e) $s50$ **(f)** number of SDs
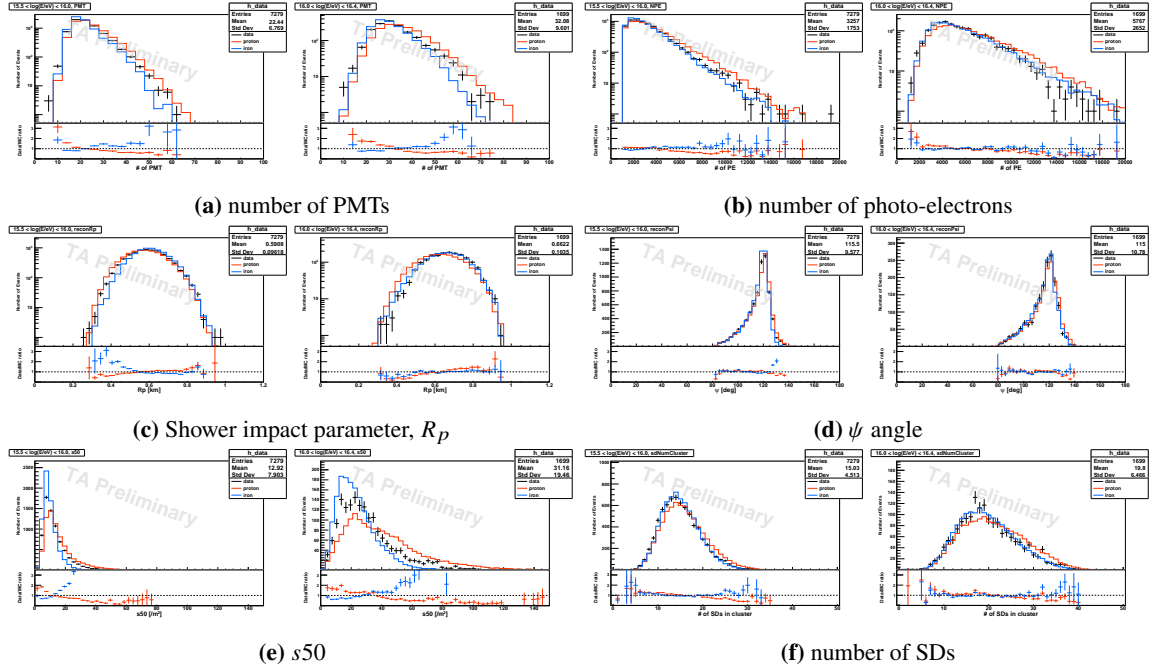
Figure 4: Data / MC comparison plots. From top left to right bottom, (a) the number of PMTs, (b) the number of photo-electrons, (c) the impact parameter, R_p [km], (d) the shower inclination angle in the shower detector plane, ψ [deg], (e) $s50$ [Mip/m^2], and (f) the number of clustering SDs are shown, respectively. Note that each parameter is divided by the energy at $\log(E/\text{eV}) = 16.0$. The black points with error bars show the data distribution, while the proton/iron MC are shown by the red/blue histograms. The MC distributions have been normalized to the same number of entries as the experimental data.

4. $X_{\max}$ Measurement

Using 540 hours of hybrid observation data, we measured the mean $X_{\max}$ ($\langle X_{\max} \rangle$) as a function of shower energy in the energy range from $10^{15.5}$ eV to $10^{16.4}$ eV. The preliminary result is shown in Figure 5a, where the black points represent the observed $\langle X_{\max} \rangle$. For comparison, the $\langle X_{\max} \rangle$ for proton and iron primaries are also plotted. The observed elongation rate was found to be $D_{10} = 15 \pm 4$ g/cm^2/decade, which is significantly smaller than the simulated values of $D_{10} = 53 \pm 2$ g/cm^2/decade for protons and 48 ± 2 g/cm^2/decade for iron primaries. In addition, we compare this result with the previously reported in [4] using TALE SD + TALE FD hybrid observations data, as shown in Figure 5b. The observed elongation rate for 10^{17} eV is consistent within statistical uncertainties for both measurements. Combining the two sets of results, we conclude that the

average mass of cosmic rays increases with energy in the range from $10^{15.5}$ eV to 10^{17} eV, followed by a reversal, where the composition becomes lighter at higher energies. This behavior may reflect a transition in the sources and propagation mechanisms of cosmic rays in these energy regimes.
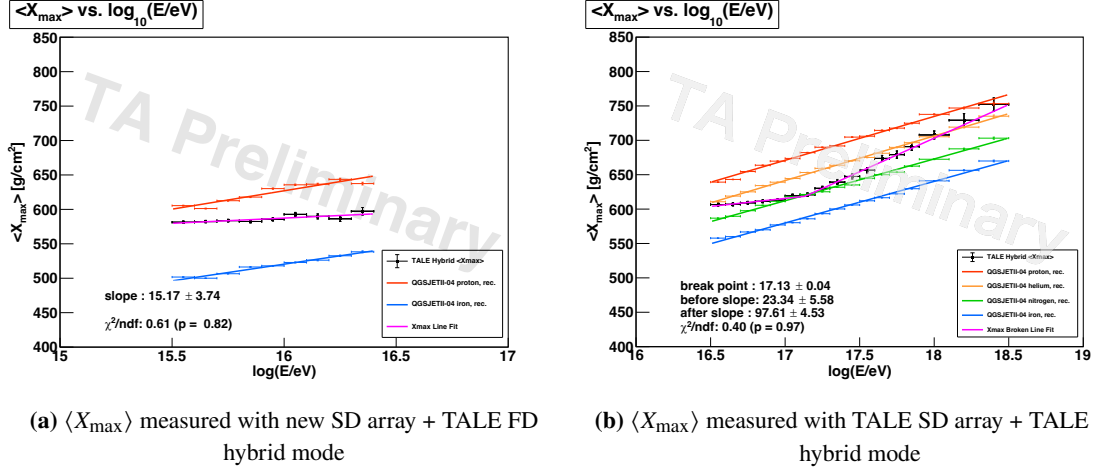

(a) $\langle X_{\max} \rangle$ measured with new SD array + TALE FD hybrid mode

(b) $\langle X_{\max} \rangle$ measured with TALE SD array + TALE FD hybrid mode

Figure 5: Preliminary results of $\langle X_{\max} \rangle$ as a function of energy. 5a: $\langle X_{\max} \rangle$ measurement by this work. For the comparison, the $\langle X_{\max} \rangle$ of proton/iron are displayed as well. 5b: Our previous $\langle X_{\max} \rangle$ measurement [4] in the energy range of $10^{16.5}$ eV to $10^{18.5}$ eV also shown for the comparison.

5. Conclusion

In this work, we presented the first preliminary results of the cosmic ray mass composition measurement using the new hybrid mode of the TALE. This new hybrid mode, which consists of a dense SD array with 100 m spacing and FD, enables precise reconstruction of air shower properties, extending the sensitivity of TALE down to the PeV energy range. Through 540 hours of hybrid observation, we measured the mean $X_{\max}$ in the energy range from $10^{15.5}$ eV to $10^{16.4}$ eV and obtained an elongation rate of $D_{10} = 15 \pm 4$ g/cm^2/decade. This result indicates the average mass composition of cosmic rays becomes heavier with increasing energy. Combining this result with previous observations using the TALE SD + TALE FD hybrid mode, we concluded that the average mass increases with energy from $10^{15.5}$ eV to 10^{17} eV, followed by a reversal to lighter compositions at higher energies. Future work will focus on increasing the observation time and improving statistical accuracy, as well as exploring primary fractions using $X_{\max}$ distributions done by the Pierre Auger Observatory in higher energies [8].

Acknowledgments

References

[1] G.V. Kulikov and G.B. Khristiansen, *Soviet Physics JETP* **35** (1959) 441.

[2] J.H. Boyer, B.C. Knapp, E.J. Mannel and M. Seman, *Nucl. Instrum. Meth. A* **482** (2002) 457.

[3] **Telescope Array** collaboration, Y. Kawachi, *PoS* **UHECR2024** (2025) 096.

[4] **Telescope Array** collaboration, K. Fujita, *PoS* **ICRC2023** (2023) 401.

[5] D. Heck, J. Knapp, J.N. Capdevielle, G. Schatz and T. Thouw (Feb, 1998).

[6] S. Ostapchenko, *Phys. Rev. D* **83** (2011) 014018 [1010.1869].

[7] **LHAASO** collaboration, Z. Cao et al., *Phys. Rev. Lett.* **132** (2024) 131002 [2403.10010].

[8] **Pierre Auger** collaboration, A. Aab et al., *Phys. Rev. D* **90** (2014) 122006 [1409.5083].

Full Authors List: The Telescope Array Collaboration

R.U. Abbasi[1], T. Abu-Zayyad[1,2], M. Allen[2], J.W. Belz[2], D.R. Bergman[2], I. Buckland[2], W. Campbell[2], B.G. Cheon[3], K. Endo[4], A. Fedynitch[5,6], T. Fujii[4,7], K. Fujisue[5,6], K. Fujita[5], M. Fukushima[5], G. Furlich[2], Z. Gerber[2], N. Globus[8*], W. Hanlon[2], N. Hayashida[9], H. He[8†], K. Hibino[9], R. Higuchi[8], D. Ikeda[9], T. Ishii[10], D. Ivanov[2], S. Jeong[11], C.C.H. Jui[2], K. Kadota[12], F. Kakimoto[9], O. Kalashev[13], K. Kasahara[14], Y. Kawachi[4], K. Kawata[5], I. Kharuk[13], E. Kido[8], H.B. Kim[3], J.H. Kim[2], J.H. Kim[2‡], S.W. Kim[11§], R. Kobo[4], I. Komae[4], K. Komatsu[15], K. Komori[16], C. Koyama[5], M. Kudenko[13], M. Kuroiwa[15], Y. Kusumori[16], M. Kuznetsov[13,17], Y.J. Kwon[18], K.H. Lee[3], M.J. Lee[11], B. Lubsandorzhiev[13], J.P. Lundquist[2,19], A. Matsuzawa[15], J.A. Matthews[2], J.N. Matthews[2], K. Mizuno[15], M. Mori[16], M. Murakami[16], S. Nagataki[8], M. Nakahara[4], T. Nakamura[20], T. Nakayama[15], Y. Nakayama[16], T. Nonaka[5], S. Ogio[5], H. Ohoka[5], N. Okazaki[5], M. Onishi[5], A. Oshima[21], H. Oshima[5], S. Ozawa[22], I.H. Park[11], K.Y. Park[3], M. Potts[2], M. Przybylak[23], M.S. Pshirkov[13,24], J. Remington[2¶], C. Rott[2,11], G.I. Rubtsov[13], D. Ryu[25], H. Sagawa[5], N. Sakaki[5], R. Sakamoto[16], T. Sako[5], N. Sakurai[5], S. Sakurai[4], D. Sato[15], S. Sato[16], K. Sekino[5], T. Shibata[5], J. Shikita[4], H. Shimodaira[5], B.K. Shin[25], H.S. Shin[4,7], K. Shinozaki[26], J.D. Smith[2], P. Sokolsky[2], B.T. Stokes[2], T.A. Stroman[2], Y. Takagi[16], K. Takahashi[5], M. Takeda[5], R. Takeishi[5], A. Taketa[27], M. Takita[5], Y. Tameda[16], K. Tanaka[28], M. Tanaka[29], S.B. Thomas[2], G.B. Thomson[2], P. Tinyakov[13,17], I. Tkachev[13], T. Tomida[15], S. Troitsky[13], Y. Tsunesada[4,7], S. Udo[9], F. Urban[30], I.A. Vaiman[13‖], M. Vrabel[26], D. Warren[8], K. Yamazaki[21], Y. Zhezher[5,13], Z. Zundel[2], and J. Zvirzdin[2]

1 *Department of Physics, Loyola University Chicago, Chicago, Illinois 60660, USA*
2 *High Energy Astrophysics Institute and Department of Physics and Astronomy, University of Utah, Salt Lake City, Utah 84112-0830, USA*
3 *Department of Physics and The Research Institute of Natural Science, Hanyang University, Seongdong-gu, Seoul 426-791, Korea*
4 *Graduate School of Science, Osaka Metropolitan University, Sugimoto, Sumiyoshi, Osaka 558-8585, Japan*
5 *Institute for Cosmic Ray Research, University of Tokyo, Kashiwa, Chiba 277-8582, Japan*
6 *Institute of Physics, Academia Sinica, Taipei City 115201, Taiwan*
7 *Nambu Yoichiro Institute of Theoretical and Experimental Physics, Osaka Metropolitan University, Sugimoto, Sumiyoshi, Osaka 558-8585, Japan*
8 *Astrophysical Big Bang Laboratory, RIKEN, Wako, Saitama 351-0198, Japan*
9 *Faculty of Engineering, Kanagawa University, Yokohama, Kanagawa 221-8686, Japan*
10 *Interdisciplinary Graduate School of Medicine and Engineering, University of Yamanashi, Kofu, Yamanashi 400-8511, Japan*
11 *Department of Physics, Sungkyunkwan University, Jang-an-gu, Suwon 16419, Korea*
12 *Department of Physics, Tokyo City University, Setagaya-ku, Tokyo 158-8557, Japan*
13 *Institute for Nuclear Research of the Russian Academy of Sciences, Moscow 117312, Russia*
14 *Faculty of Systems Engineering and Science, Shibaura Institute of Technology, Minato-ku, Tokyo 337-8570, Japan*
15 *Academic Assembly School of Science and Technology Institute of Engineering, Shinshu University, Nagano, Nagano 380-8554, Japan*
16 *Graduate School of Engineering, Osaka Electro-Communication University, Neyagawa-shi, Osaka 572-8530, Japan*
17 *Service de Physique Theorique, Universite Libre de Bruxelles, Brussels 1050, Belgium*
18 *Department of Physics, Yonsei University, Seodaemun-gu, Seoul 120-749, Korea*
19 *Center for Astrophysics and Cosmology, University of Nova Gorica, Nova Gorica 5297, Slovenia*
20 *Faculty of Science, Kochi University, Kochi, Kochi 780-8520, Japan*
21 *College of Science and Engineering, Chubu University, Kasugai, Aichi 487-8501, Japan*
22 *Quantum ICT Advanced Development Center, National Institute for Information and Communications Technology, Koganei, Tokyo 184-8795, Japan*
23 *Doctoral School of Exact and Natural Sciences, University of Lodz, Lodz, Lodz, 90-237, Poland*
24 *Sternberg Astronomical Institute, Moscow M.V. Lomonosov State University, Moscow 119991, Russia*
25 *Department of Physics, School of Natural Sciences, Ulsan National Institute of Science and Technology, UNIST-gil, Ulsan 689-798, Korea*
26 *Astrophysics Division, National Centre for Nuclear Research, Warsaw 02-093, Poland*
27 *Earthquake Research Institute, University of Tokyo, Bunkyo-ku, Tokyo 277-8582, Japan*
28 *Graduate School of Information Sciences, Hiroshima City University, Hiroshima, Hiroshima 731-3194, Japan*
29 *Institute of Particle and Nuclear Studies, KEK, Tsukuba, Ibaraki 305-0801, Japan*
30 *CEICO, Institute of Physics, Czech Academy of Sciences, Prague 182 21, Czech Republic*

* Presently at: KIPAC, Stanford University, Stanford, CA 94305, USA
† Presently at: Purple Mountain Observatory, Nanjing 210023, China
‡ Presently at: Physics Department, Brookhaven National Laboratory, Upton, NY 11973, USA
§ Presently at: Korea Institute of Geoscience and Mineral Resources, Daejeon, 34132, Korea
¶ Presently at: NASA Marshall Space Flight Center, Huntsville, Alabama 35812, USA
‖ Presently at: Gran Sasso Science Institute, 67100 L'Aquila, L'Aquila, Italy